24th INTERNATIONAL CONGRESS ON SOUND AND VIBRATION
23–27 July 2017, London

ICSV24
23-27JULY 2017
LONDON CALLING

FAR FIELD SOUND FROM HIGH SPEED VIDEO FOOTAGE

John Lamb, Daniel Zheng and Nicolas Etaix
Dyson Technologies Ltd. Tetbury Hill, Malmesbury, UK
email: john.lamb@dyson.com

It has recently been demonstrated that high speed video imaging can be used to extract surface velocity profiles at sufficiently high frame rates to be useful for vibro-acoustic purposes. Use of video imaging is potentially valuable for light weight structures where the addition of accelerometers can significantly modify the modal response. As the video based approach can capture images of the complete vibrating surface in every frame, it can potentially be used to track transient and steady state behaviour without requiring reference measurements.

In this work, high speed video footage is used to determine the modal response of a resilient spherical cap attached to a spherical motor housing. The velocity profile extracted from the video footage is used as input into a numerical simulation and the far field sound pressure level of the vibrating system is calculated. The simulation results are compared to experimental measurements.

Keywords: High speed video, vibro-acoustics

1. Introduction

Characterising vibration induced noise from acoustic measurements can be difficult, particularly when measuring a machine under operating conditions where it can be impractical to completely isolate airborne or aero-dynamically induced noise from that induced by vibration. Rather than perform acoustic measurements it is possible to measure the surface vibration and infer the pressure field radiated by the source. The advantage of this approach is that the resulting estimate is free of any airborne contributions. For well known systems is it possible to estimate far field pressures from a relatively coarse grid of vibration measurements [1, 2], however for general cases, accurate predictions require a large number of vibration measurements to be made. Traditional approaches to measuring the response of a vibrating surface make use of surface mounted accelerometers. When high numbers of accelerometers are used to measure surface vibration the process can be very time consuming while the influence of the added weight of the instrumentation can modify the vibration behavior. This is especially true for light weight structures. Scanning laser vibrometers provide a non-contact method for measuring surface vibration and have been used successfully to predict the sound radiation from a vibrating a surface [3]. The equipment required for raster scanning laser vibrometry is, however, very expensive. Video based techniques for tracking movement and vibration have been suggested as an ideal non-contact [4] approach. In recent years, high frame rate, high resolution video cameras and the computer processing power necessary to analyse the resulting data have become increasingly accessible making this approach within reach of noise control engineers.

In this work we build on recent results exploring the use of high speed video to amplify and track sub-pixel level motion for the determination of vibration modes and audio signal extraction. Phase based video magnification techniques were introduced by Wadhwa et al [5] which allow for robust amplification of small motions within video frames. Through the use of a high speed camera, Davis et al. [6] were able to demonstrate that motion amplification could be used to measure micron level

displacements induced on everyday objects by the fluctuating pressure field of an incident sound wave. They were able to successfully extract intelligible speech from the vibration response of a surface excited by a nearby talker. These techniques have also been extended to monitor the vibration modes and material parameters of vibrating structures [7, 8]. In these previous works, the motion of the vibrating object was assumed to be fixed within a single plane. Perspective correction was applied by Hopper et al. [9] to account for the angle and distance of a given image feature with respect to the camera. In this way, the motion amplification technique was used to successfully extract the 2D mode shapes of vibrating plates.

In this paper the authors extend the perspective correction technique to the curved shell of the spherical motor housing of a Dyson vacuum cleaner, as shown in fig. 1a and 1b. The resulting vibration profile is then used to estimate the amplitude of the pressure field. The curved shell is of particular interest as it provides a test bed for a more complicated geometry than previously investigated. The spherical geometry also admits analytic investigation.

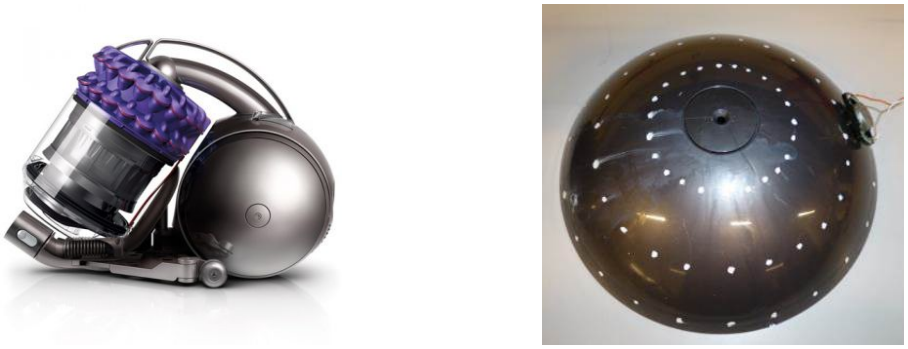

(a) Image of a Dyson vacuum cleaner with a spherical motor housing.

(b) The spherical cap removed from the product.

Figure 1: Photographs of the spherical cap in situation and in isolation.

2. Small motion amplification

It has been suggested for some time that video based monitoring techniques offer an ideal non-contact method of measuring surface vibrations [4]. To be practical for noise estimation purposes the video frame-rate must be sufficiently high to satisfy the Nyquist criterion at the frequency of interest and the image resolution must be high enough to resolve the displacement associated with the surface vibrations. Even with the advent of high resolution digital video cameras, the displacement of a vibrating surface can be too subtle to be revealed from the raw video footage alone.

Recently, video motion amplification processing algorithms have been developed which allow variations between video frames to be magnified without a concurrent increase in noise [5]. This technique is based on phase magnification of a wavelet decomposition of the image. Individual wavelets are tracked frame to frame and relative phase differences between wavelets in subsequent frames are amplified. The phase amplification shifts the relative location of the wavelet along its principle axis which, upon reconstruction of the image, results in magnification of the underlying motion. Temporal band-pass filters can be employed to ensure that motion is amplified only at specific frequencies. This can be useful for revealing resonant modes of the system [7] and has been demonstrated to work even in the presence of broad-band excitation signals [9]. The amplitude of the magnified motion in the reconstructed image frame has been shown to increase linearly with amplification factor α and displacement estimates derived from these provide accuracy on par with traditional accelerometer and laser vibrometer based methods [7, 8, 9].

3. Perspective correction

The motion amplification technique operates in the plane of the image frame. Any motion into or out of the image plane cannot be revealed even with extensive motion amplification applied. To extract the displacement of 2D mode shapes Hopper et al. [9] imaged a vibrating plate at an angle, which ensured components of the displacements normal to the surface of the plate were captured within the image plane. A perspective correction was necessary to back project the imaged displacement to a quantity normal to the surface of the plate. In this work we aim to characterize the vibration and subsequent sound radiation of a plastic shell cover attached to a spherical motor housing shown in fig. 1a and fig. 1b. Apart from at the centre of the shell, the curved surface provides a natural angle with an on-axis video camera to ensure that the radial displacement always has components in the image frame. The geometry and nomenclature for this system is defined in fig. 2.

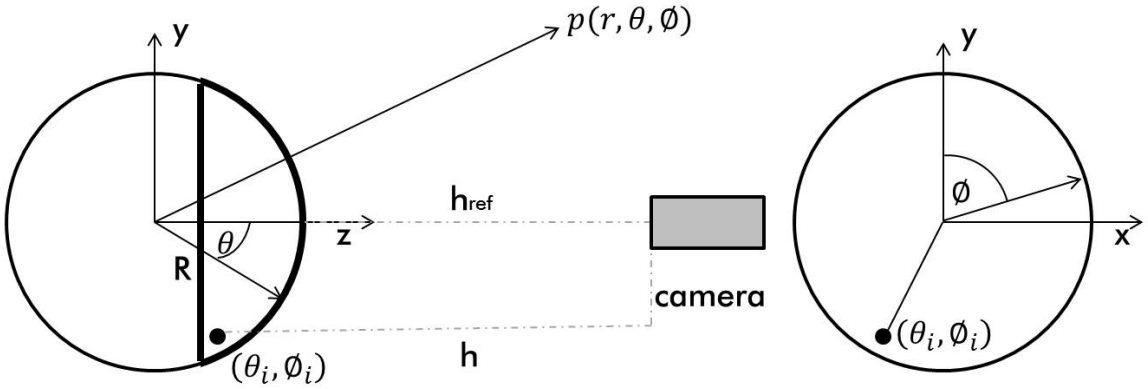

Figure 2: Schematic diagram providing the co-ordinate system and naming conventions used within this work.

The perspective correction used to determine the displacement d normal to the surface of the sphere is a simple trigonometric expression combined with a correction to account for the relative depth of different features within the image frame.

$$d = \frac{h}{h_{ref}} \frac{d'}{\sin(\theta_i)} \tag{1}$$

where $d' = \sqrt{x^2 + y^2}$ is the magnitude of the displacement in the x and y plane and h_{ref} is the distance from the camera to the plane containing the reference feature with a known size. The size of the reference feature can be measured in pixels and used to convert the displacement measured from the video post-processing into an absolute value.

A displacement profile $d(\theta_i, \phi_i, t)$ is obtained by independently tracking image features over the surface of the vibrating system. Assuming a linear system with harmonic excitation the velocity profile may be recovered from the first differential of the displacement data. In this work the data is processed in the frequency domain and the vibration profile is given by

$$V(\theta_i, \phi_i, \omega) = -i\omega \text{FFT}\left(d(\theta_i, \phi_i, t)\right). \tag{2}$$

4. Sound field estimation

The shell, which serves as a wheel during operation, is attached to the motor housing at its centre and is free to move at its rim. Here we consider the motor housing and shell as a single continuous sphere. Under this assumption, the sound produced by the vibration of the shell can be modeled as

resulting from a velocity distribution over the surface of our model sphere. The free-field pressure generated by an arbitrary continuous vibration profile on a sphere has a closed form solution [10, 11]. The pressure may be calculated using eq. (3) where the explicit time dependence has been dropped for brevity.

$$p(r,\theta,\phi) = i\rho c \sum_{n=0}^{\infty} \sum_{m=-n}^{n} A_{nm} Y_n^m(\theta,\phi) \frac{h_n^{(2)}(kr)}{h_n^{(2)'}(kR)}, \tag{3}$$

where c is the speed of sound, ρ is the density of air, $h_n^{(2)}(kr)$ the spherical Hankel function of the second kind of order n where n is an integer, k is the wavenumber, r is the distance from the centre of the sphere to the measurement position, R is the radius of the sphere, the prime indicates the first derivative and $Y_n^m(\theta,\phi)$ are the spherical harmonics

$$Y_n^m(\theta,\phi) = P_n^m(cos\theta)e^{(im\phi)}, \tag{4}$$

with $P_n^m(.)$ representing the associated Legendre polynomials. The A_{nm} are the amplitude coefficients of each term in the series. By the orthogonality of the spherical harmonics the expansion coefficients are uniquely related to the velocity profile $V(\theta_i,\phi_i)$ on the surface of the sphere

$$V(\theta_i,\phi_i) = \sum_{n=0}^{\infty} \sum_{m=-n}^{n} A_{nm} P_n^m(\cos\theta_i) e^{(im\phi_i)}. \tag{5}$$

The A_{nm} may be approximated using a truncated series, calculation of which can be realised by recasting eq. (5) as a matrix and solving this system of equations in a least mean squared sense with a suitable numerical package.

$$\begin{bmatrix} Y_0^0(\theta_1,\phi_1) & Y_1^1(\theta_1,\phi_1) & \dots & Y_N^{-N}(\theta_1,\phi_1) \\ Y_0^0(\theta_2,\phi_2) & Y_1^1(\theta_2,\phi_2) & \dots & Y_N^{-N}(\theta_2,\phi_2) \\ \vdots & \vdots & \ddots & \vdots \\ Y_0^0(\theta_I,\phi_I) & Y_1^1(\theta_I,\phi_I) & \dots & Y_N^{-N}(\theta_I,\phi_I) \end{bmatrix} \times \begin{bmatrix} A_{0,0} \\ A_{1,1} \\ \vdots \\ A_{N,-N} \end{bmatrix} = \begin{bmatrix} V(\theta_1,\phi_1) \\ V(\theta_2,\phi_2) \\ \vdots \\ V(\theta_I,\phi_I) \end{bmatrix} \tag{6}$$

The series truncation is typically performed to ensure that N is sufficiently high for the sum to converge to a predetermined tolerance. The number of measurements required to fully determine the matrix grows as $n^2+n+m+1$ meaning that in order to resolve high order harmonics on the sphere, a very dense grid of measurements is required.

5. Experimental configuration

The photographs in fig. 3 show the layout of the experiments for capturing the high speed video footage and acoustics. An IDT MotionPro Y4-S2 high speed camera was used to record the system vibration. A total of 69 white dots were painted onto the shell as tracking markers. A bright light source was required to maintain sufficient contrast between the markers and the background at high frame rates. Care was required to prevent glare in the camera image obscuring the tracking features. A typical image captured by this configuration is shown in fig. 4.

An external exciter was used to provide a controllable vibration source and can be seen in fig. 4 located near the 6 O'clock position towards the outer rim of the shell (green square). An accelerometer is also shown (red circle) at the 12 O'clock position and was included to serve as an accuracy reference as well as a global reference for the subsequent acoustic measurements.

The system was raised up from the floor by a few cm to ensure the shell cap was free to vibrate. To determine the vibration modes of the system a B&K type 8206 impact hammer was used to impact the shell close to the position of the shaker. The first few peaks in the resulting transfer function were

(a) Photograph of the high speed video experiment.

(b) Photograph of the experimental configuraiton used in the hemi-anechoic chamber.

Figure 3: Photographs of the experimental configurations used to measure the data.

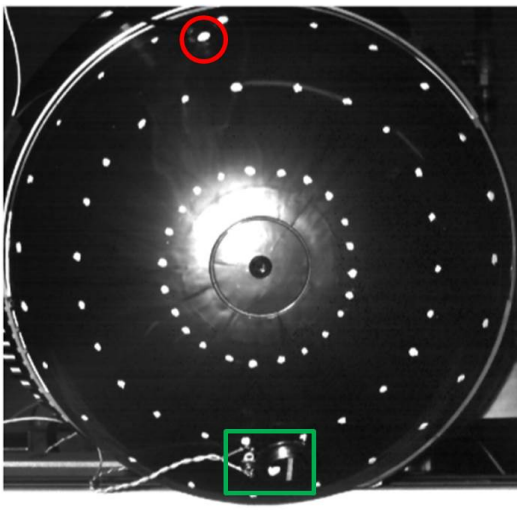

Figure 4: A typical video frame displaying the high contrast dots. A red circle has been drawn around the accelerometer and green square around the vibration shaker.

used to infer the resonant frequencies of the shell. Video footage was captured at four frequencies referred to in the following as modes 1 to 4.

5.1 Acoustic measurements

The acoustic measurements were not captured simultaneously with the video footage as the cooling fans of the high speed camera generated significant noise. Instead, separate experiments were conducted in a hemi-anechoic chamber using a 10 microphone hemisphere on a 2 m radius in accordance with IEC 60704-2-1 [12]. The motor housing was placed centrally in the microphone array as shown in fig. 3b. The exciter was driven at the same modal frequencies used during the video capture. The pressure at each microphone was recorded and the mean sound pressure level determined. The acceleration level of the reference accelerometer was also recorded. Linear behaviour was assumed, allowing the acceleration level to be used to relate the acoustic measurements to the previously recorded video footage.

5.2 Video amplification and motion tracking

The video recording was made at a resolution of 983 by 980 pixels and a frame rate of 1000 Hz with a total of 200 frames captured per test. Post-processing was conducted in Matlab. Motion amplification was applied to the video sequence. It was found that a combination of different amplification levels was required to achieve the best compromise between noise and the introduction of artefacts for each concentric ring of tracking points. For mode 1 amplification factors of 5, 25 and 50 were applied to the outer, middle and inner rings of measurement points respectively, see fig. 4 for reference.

To track the motion of the individual points, a threshold was applied to the grey scale video to separate the tracking dots from the background. Then the x and y co-ordinates of the centroid of each dot was calculated for each video frame and stored as vectors in x and y. The perspective correction as discussed in section 3 was applied to this data and the normal velocity profile across the spherical shell was computed. The resulting velocity profile is shown in fig. 5a.

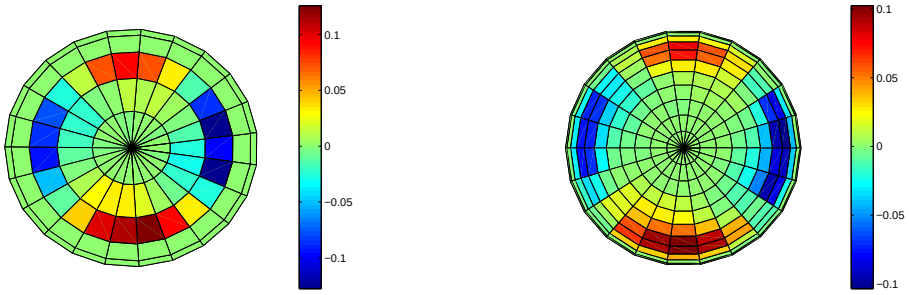

(a) Velocity profile as inferred from the video post processing for mode 1.

(b) Reconstructed velocity profile for N = 20.

Figure 5: The measured and reconstructed (N = 20) velocity profiles for the vibrating shell (mode 1). The colour scale is in ms^{-1}

6. Results

To understand how accurately the velocity profile could be recovered, the acceleration level measured by the accelerometer was converted to a displacement and compared to the displacement inferred from the amplified video motion. The displacements for all four modes are shown in table 1. For mode 1 the agreement is very good, however, the agreement is very poor for modes 2-4. No obvious modal behaviour could be observed for these modes in the amplified videos, suggesting that the motion was below the noise floor of the video capture system.

Table 1: Table showing the calculated displacements for the four vibration modes chosen for investigation.

Mode	Accelerometer displacement (mm)	Video displacement on-axis (mm)
1	0.102	0.105
2	0.004	0.0004
3	0.008	0.0005
4	0.001	0.0003

6.1 Sound pressure level estimates

The measured vibration profile (mode 1) was used to estimate the coefficients A_{nm} using the Matlab backslash operator to solve the system of equations in eq. (6). $V(\theta_i, \phi_i)$ was set to zero for all locations where no video tracking had been performed on the assumption that there was no vibration at these positions. The system was solved up to order N = 20, which required interpolation of the measured data onto a larger grid of 23 by 23 points. The reconstructed velocity profile using the estimated A_{nm} is shown in fig. 5b. Using eq. (3) the free field pressures at 10 positions equivalent to the experimental microphone locations were calculated. The mean value for the sound pressure level over the 10 positions is shown in table 2 along with the equivalent value for the measured data.

An FEA simulation was also performed using COMSOL. The vibration profile inferred by the video footage was used to define the surface velocity of a spherical geometry. The numerical simulation provides a useful reference to the analytic simulation for free-field radiation. The COMSOL model is also more flexible in that it allows the effects of the reflective floor of the hemi-anechic chamber (half-space) to be simulated. Results of the FEA simulations with and without the reflective boundary are also given in table 2.

Table 2: Table summarising the measurement and simulation results for the acoustic emission of mode 1.

Mode	Acoustic measurement dB re 20 μPa	Analytical simulation free-field dB re 20 μPa	FEA simulation free-field dB re 20 μPa	FEA simulation half-space dB re 20 μPa
1	37	58	57	62

7. Discussion

The reference accelerometer displacement estimate agreed well with the estimated displacement derived from the video footage for mode 1. This is in line with the findings of other authors, giving confidence that the use of video techniques is valid for the extraction of mode shapes on even complex geometries.

Only the largest of the vibration modes was recoverable using the video magnification technique. The amplitude of the vibration for the other modes was below the noise floor of the video measurement system. It is worth stating that the displacement levels determined from the accelerometer values for modes 2-4 corresponded to approximately one thousandth of a pixel in this study.

The sound pressure level estimates of both the analytical and FEA simulations are in very poor agreement with the actual measured results. The fact that the free-field analytic and FEA simulations show similar results is encouraging and suggests that the simulations failed to accuratly reflect the experiment. One obvious oversimplification was the assumption that the spherical shell was continuous with the body of the sphere. In reality the edge of the shell is free and sound will be radiated from the rear as well as from the front of the structure, 'dipole' like radiation. Being in a regime where $ka \ll 1$, the influence of the rear radiation is likely to be significant.

8. Conclusions

High speed video footage with a simple perspective correction was shown to be successful in determining the surface vibration profile of a curved geometry.

A spherical model was assumed and the vibration of the shell was mapped to a velocity profile on a sphere. An analytic model and an FEA model were used to calculate the resulting sound pressure

field and compared to experimental data for the sound pressure levels on a 2 m hemisphere. The analytical and numerical simulations were in reasonable agreement, however they provided a poor estimate of the actual measured sound pressure levels. This is most likely due to oversimplification of the simulations in failing to account for the rear radiation of the vibrating shell.

REFERENCES

1. Daniel Taylor and John Lamb. Assessing the vibro-acoustic radiation characteristics of a compact consumer appliance. *Proc. 45th International Congress and Exposition on Noise Control Engineering (Internoise 2016)*, pages 7513–7523, 2016.

2. DD ISO/TS 7849-2:2009. Acoustics- determination of airborne sound power levels emitted by machinery using vibration measurement - Part 2: Engingeeing method including the determination of the adequate radiation factor. *ISO Standard*, 2009.

3. G. Revel and G. Rossi. Sound power estimation by laser doppler vibration measurement techniques. *Journal of Shock and Vibration*, 5(5/6):297–305, 1998.

4. C.K. Lee and W. Faig. Vibration monitoring with video cameras. *International Archives of Photogrammetry and Remote Sensing.*, 31(B5):152:159, 1996.

5. Neal Wadhwa, Michael Rubinstein, Fredo Durand, and William T. Freeman. Phase based video magnification. *Computer Vision and Pattern Recognition*, 32(4):Article 80, 2013.

6. Abe Davis, Michael Rubinstein, Neal Wadhwa, Gautham Mysore, Fredo Durand, and William T. Freeman. The visual microphone: Passive recovery of sound from video. *ACM Transactions on Graphics (Proc. SIGGRAPH)*, 33(4):79:1–79:10, 2014.

7. Justin G. Chen, Neal Wadhwa, Yong jin Cha, Fredo Durand, William T. Freeman, and Oral Buyukozturk. Modal identification of simple structures with high-speed video using motion magnification. *Journal of Sound and Vibration*, 345:58–71, 2015.

8. Abe Davis, Katherine L. Bouman, Justin G. Chen, Michael Rubinstein, Fredo Durand, and William T. Freeman. Visual vibrometry: Estimating material properties from small motions in video. *IEEE Transactions on Pattern Analysis and Machine Intelligence*, PP(99), 2016.

9. H. Hopper, D. Zheng, R. Faventi, and S.R. Voisey. Measurement of 2D vibration modes using amplification of high speed video in the presence of noise. *Proc. 42nd Int. Conf. on Acoustics, Speech and Signal Processing*, pages 1637–1641, 2017.

10. R.M. Aarts and J.E.M. Janssen. Sound radiation from a resilient spherical cap on a rigid sphere. *Journal Acoust. Soc. Am.*, 127(4):2262–2273, 2010.

11. P.M. Morse and K.U. Ingard. *Theoretical Acoustics*. Princeton University Press, 1986.

12. IEC 60704-2-1. Household and similar electrical appliances - Test code for the determination of airborne acoustical noise - Part 2-1: Particular requirements for vacuum cleaners. *IEC Standard*, 2001.